P1.20 THE IDENTIFICATION AND VERIFICATION OF HAZARDOUS CONVECTIVE CELLS OVER OCEANS USING VISIBLE AND INFRARED SATELLITE OBSERVATIONS[†]

Michael F. Donovan*
Earle R. Williams
Massachusetts Institute of Technology Lincoln Laboratory, Lexington, MA

Cathy Kessinger, Gary Blackburn, Paul H. Herzegh
National Center for Atmospheric Research, Boulder, CO

Richard L. Bankert, Steve Miller
Naval Research Laboratory, Monterey, CA

Frederick R. Mosher
Applied Aviation Sciences
Embry-Riddle Aeronautical University, Daytona Beach, FL

1. ABSTRACT

Three algorithms based on geostationary visible and infrared (IR) observations, are used to identify convective cells that do (or may) present a hazard to aviation over the oceans. The algorithms were developed at the Naval Research Laboratory (NRL), National Center for Atmospheric Research (NCAR), and Aviation Weather Center (AWC). The performance of the algorithms in detecting potentially hazardous cells is determined through verification based upon data from National Aeronautical and Space Administration (NASA) Tropical Rainfall Measuring Mission (TRMM) satellite observations of lightning and radar reflectivity, which provide internal information about the convective cells. The probability of detection of hazardous cells using the satellite algorithms can exceed 90% when lightning is used as a criterion for hazard, but the false alarm ratio with all three algorithms is consistently large (~40%), thereby exaggerating the presence of hazardous conditions. This shortcoming results in part from limitations resulting from the algorithms' dependence upon visible and IR observations, and can be traced to the widespread prevalence of deep cumulonimbi with weak updrafts but without lightning, whose origin is attributed to pronounced departures from non-dilute ascent.

2. INTRODUCTION

Continental convection hazardous to aviation has received much attention in numerous field programs over several decades, beginning with the Thunderstorm Project (Byers and Braham, 1949). This pioneering study called early attention to the thunderstorm as the most hazardous convective form. This and subsequent investigations have relied heavily on aircraft, radar and lightning observations to effectively probe the internal dynamic, microphysical and electrical structure of thunderstorms. The updraft is a key internal variable in its influence on many aviation hazards (turbulence, icing, hail, and lightning). These internal measurements are generally augmented with satellite observations – an important surveillance tool, but one that reveals only the exterior characteristics of clouds (e.g., IR cloud temperature, cloud height), owing to the opaque nature of moist convection in the visible and infrared region.

The present study shifts the focus in hazardous weather from land to ocean, where conditions are notably more benign, but data much more limited. The challenge undertaken here is the remote identification of hazardous oceanic convective cells, but without the critical benefit of routine surveillance by radar and lightning detection systems, which provide crucial information on the structure and processes interior to the cells. The mainstay of oceanic weather surveillance is the international fleet of geostationary satellites that operate in the visible and infrared. We examine three recently developed convective diagnostic algorithms that rely upon geostationary data to meet operational needs for detection of hazardous cells. The verification of

[†]This work was sponsored by the Federal Aviation Administration under Air Force Contract FA8721-05-C-0002. Opinions, interpretations, conclusions, and recommendations are those of the authors and are not necessarily endorsed by the United States Government.

[*]*Corresponding author address*: Michael F. Donovan, MIT Lincoln Laboratory, 244 Wood Street, Lexington, MA 02420-9185; e-mail: miked@ll.mit.edu

convection and its hazard potential is achieved through analysis of simultaneous observations of convective cell interiors (radar reflectivity, lightning) obtained by the NASA TRMM satellite in Low Earth Orbit (LEO). The three algorithms evaluated here were developed by NRL, NCAR, and AWC under funding by the Aviation Weather Research Program (AWRP) of the Federal Aviation Administration (FAA).

A long-recognized contrast between continental and oceanic convection lies in the nature of the underlying surface. A water surface resists heating by sunlight relative to land, both because of its higher heat capacity and its tendency to mix with deeper water. This contrast affects the updraft speed at cloud base. But the existence of updraft is a basic ingredient of an electrification process that appears to be the same for land and ocean. For example, Takahashi (1978) has documented tall oceanic clouds with low lightning activity, but with electrical structure and electrically charged graupel particles similar to continental storms.

In summary, extensive satellite intercomparisons on hundreds of storm cells demonstrate here that geostationary satellite observations show considerable skill in identifying oceanic convection. The intercomparisons have also revealed substantial imperfection in that hazardous convection is over-predicted by the algorithms. This shortcoming is a natural result of the non-unique relationship between cloud height and updraft speed. The prevalence of deep clouds with modest updraft speed over the oceans is interpreted as a systematic departure from non-dilute ascent in oceanic convection (Zipser, 2003).

The present study is not the first of its kind, and the interest in oceanic convection is on the rise as intercontinental routes expand. Work by Mahoney et al. (2000) and Martin et al. (2005) have also been concerned with the scoring and validation of one of three algorithms under consideration here (AWC).

Section 3 is concerned with detailed descriptions of the three algorithms for convective diagnosis, and Section 4 details the observational capabilities of the TRMM satellite used to verify thunderstorms and hazardous cells. Section 5 defines specific terminology used in the study and Section 6 describes the findings and statistical results in three separate satellite intercomparisons over a period of three years. The discussion and interpretation of these results is found in Section 7, followed by the Conclusions in the final section.

3. SATELLITE-BASED DETECTION ALGORITHMS

Three algorithms for convective diagnosis have been implemented for operational trials by the AWRP Oceanic Weather Product Development Team (OW PDT). Each uses data from the Geostationary Operational Environmental Satellites (GOES) and is designed to distinguish benign cloud regions from deep convection that is potentially hazardous to aviation.

3.1 Cloud Top Height (CTOP) Product

The objective of the Cloud Top Height (CTOP) product is to determine and display the heights of clouds. Originally developed by NRL (Miller et al., 2005) and later re-implemented by NCAR for OW PDT use, the product indicates the presence of deep convection and other cloud features over a range of flight level altitudes. The product is currently scheduled to become operational in 2008 and thereafter serve to advise pilots, dispatchers and air traffic controllers on the presence of deep convection and other cloud types on a global scale (Herzegh et al., 2002). The product is currently generated in real-time for three large domains - the central Pacific Ocean, northern Pacific Ocean and the Gulf of Mexico. Coverage for the North Atlantic Ocean is scheduled to begin in 2007-08.

Production of the CTOP product begins with projection of the 11 micron channel satellite brightness temperature data onto an equidistant cylindrical latitude-longitude grid. Over the vast Pacific Ocean, data from both the GOES-9 and GOES-10 satellites are required to complete this coverage. In regions where the satellites overlap each other, the data are mosaicked. Due to variations in satellite scanning strategies and update rates, old data are replaced with the most recently received data at 20 minute intervals. If no new data are received within the 20 minute update period, the previous data are used. Data from the GOES-12 are used to cover the Gulf of Mexico domain with an update interval of 30 minutes. No mosaic is required for the latter domain.

The next step is to acquire sounding data from the National Center for Environmental Prediction (NCEP) Global Forecast System (GFS) numerical model. The model data, at a 1°x1° horizontal resolution, are transferred to the same map projection as the IR temperature grid. The column of model temperature and pressure values nearest

each satellite temperature grid point is then used to make a vertical profile. The satellite temperatures are matched with the profile data to determine the equivalent pressure level. Lastly, the pressure levels are converted to flight level altitudes above sea level using the standard atmosphere assumption to be consistent with aviation usage. Figure 1 shows an example of the CTOP product over the Gulf of Mexico where numerous convective cells have developed from south of Cuba to the Bahamas Islands. Warmer colors represent higher cloud top heights. Deep convection showing contour levels greater than or equal to 40,000 ft denote potential aviation hazards.

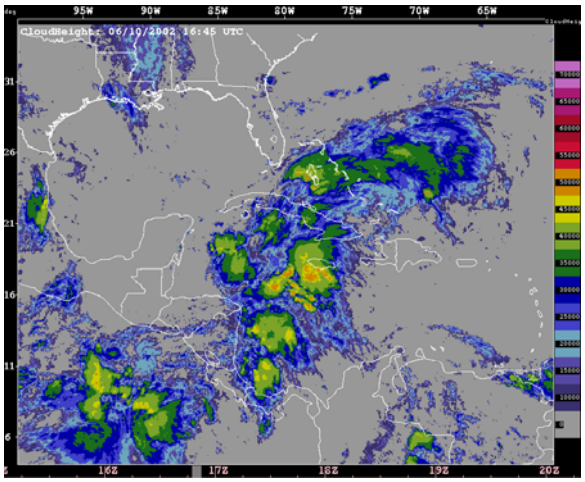

Figure 1. The Cloud Top Height product for convection observed over the Gulf of Mexico on 10 June 2002 at 16:45 UTC. Cloud top heights (feet) are shown in intervals of 5,000 feet and gray areas denote clear sky. Cloud heights greater than or equal to 40,000 feet (light green) denote clouds associated with potential hazards to aviation.

3.2 Cloud Classification (CC) Product

The NRL Cloud Classification (CC) algorithm (Tag et al., 2000) is another product that is used by the OW PDT to assist in the accurate detection of deep convective clouds. The CC product classifies satellite imagery into several cloud types or layers and has been optimized to provide coverage over the western Atlantic Ocean, continental United States and eastern Pacific Ocean.

Training sets were based on all combinations of GOES-8/10, day/night (as defined by the solar zenith angle), and land/ocean samples where collective agreement was reached among three independent experts interpreting the samples. These data were drawn from thousands of 16x16 km (day) and 32x32 km (night) samples created from GOES-8 and GOES-10 scenes. All GOES-8 samples were adjusted to better emulate the GOES-12 data that now covers the GOES-8 former Atlantic domain.

Over 100 characteristic features were computed or extracted from each of the training samples using all GOES channels during the day and all but the visible channel at night. The feature set is subsequently reduced by applying a feature selection algorithm to the training data for each classifier resulting in 10 to 15 features that maximize classification accuracy. Various classes are identified (i.e., cirrus, stratus, etc. for daytime and thin/thick high, low, etc. for nighttime) but of interest in the present study are the cumulonimbus (Cb) and cirrostratus associated with deep convection (CsAn) classes (for daytime classifications) and the deep convection (DC) class (for nighttime classifications).

The CC algorithm is a 1-nearest neighbor classifier with each sample within an image given the same class as the training sample it most closely resembles (minimum Euclidean distance) within the feature space. All satellite pixels within the sample are assigned the same class. Satellite sample boxes overlap each other such that pixels are classified four times except near the image edges. The final classification of the pixel becomes the simple majority. An example of a daytime classification image over the central and eastern United States and neighboring oceanic regions is shown in Figure 2. The daytime classifier delineates among several cloud types as is evident between the mid-layer altostratus (As) and high thin cirrostratus (Cs) and cirrocumulus (Cc) clouds observed in south central Canada and the vertically developed clouds (CsAn and Cb) associated with air mass thunderstorms over Missouri and Arkansas.

3.3 Global Convective Diagnostic (GCD)

A third experimental algorithm designed to detect deep convection and thunderstorms was developed at the AWC (Mosher, 2002). The algorithm computes the satellite temperature difference between the 6.7 micron water vapor channel and the 11 micron infrared channel to identify deep convection. The diagnostic product is produced globally since all geostationary satellites contain these two channels.

The premise behind the algorithm is that in areas of active uplift within deep convective clouds, moisture and cloud particles are being lifted to the top of the troposphere. In these regions, the satellite

measurements of infrared and water vapor temperatures have very similar values and can be used to identify potentially turbulent areas associated with thunderstorm updrafts. As the clouds encounter strong upper level winds, the cirrus cloud particles are blown downwind and begin to descend under gravity but the water vapor remains at the same altitude. Thus the satellite senses a larger temperature difference between the colder water vapor temperature and the warmer cloud particle temperature. The algorithm eliminates any cloudy region from a hazardous convective category wherever the infrared temperature is warmer than the water vapor temperature by 1° C or more.

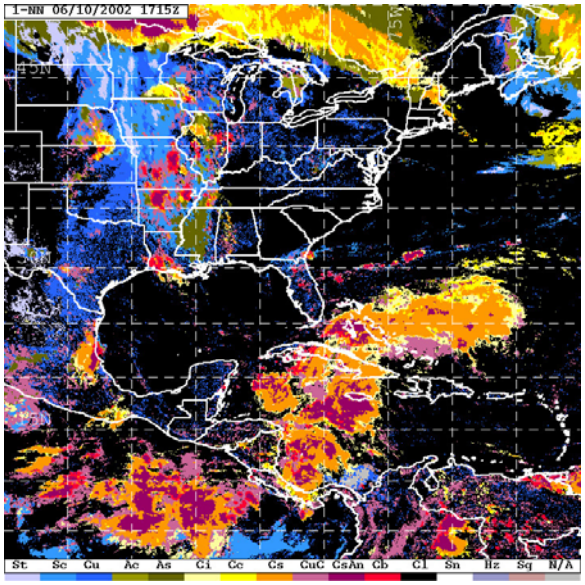

Figure 2. The daytime Cloud Classification product for clouds observed over the central and eastern United States and neighboring oceanic regions on 10 June 2002 at 17:15 UTC. Diagnosis of potentially hazardous clouds containing vertical development is shown as magenta (CsAn) and red (Cb).

There are other situations where cirrus cloud formation not associated with thunderstorms can be mistakenly detected by the algorithm (i.e., wind motions near jet streams and within mid latitude storm development). In practice, the application of the GFS model 4 layer Lifted Index (LI) stability product has shown promise in eliminating these instances. The GCD algorithm utilizes the LI product to eliminate all areas where the LI values are greater than 1° C, indicating stable atmospheric conditions.

The GCD algorithm maps the temperature difference between the water vapor and infrared channels on a global scale with a 30-minute update rate. Merging techniques are applied to reconcile areas of overlapping satellite coverage and time skew among the suite of geostationary satellite samples. The final product is a composite diagnostic that highlights as 'convective' all areas not eliminated by the stability filter. The spatial resolution is 10 km. Figure 3 illustrates the GCD product (depicted with a red color) overlaid on the infrared composite over the entire globe. Note the presence of deep convection in the Southern Hemisphere, particularly in Africa and along the Inter Tropical Convergence Zone (ITCZ) in the Central Pacific and Indian Oceans and the general absence of convection in the Northern Hemisphere.

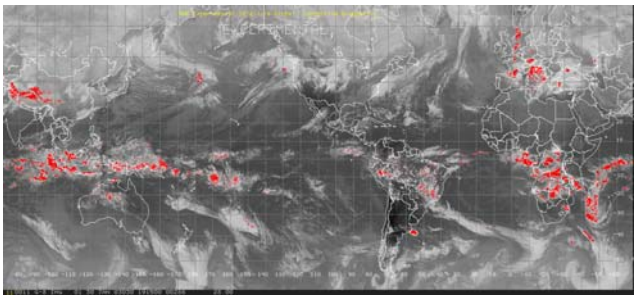

Figure 3. The Global Convective Diagnostic product. Areas of deep convection are identified as red. Data were collected from 30 January 2003 near 19:15 UTC.

4. ALGORITHM VERIFICATION: USE OF TRMM PRODUCTS

Orbiting the Earth at a 35° inclination angle, the TRMM satellite was designed to procure information on the global distribution of rainfall and heat exchange in the tropics. Observations from its Visible and Infrared Radiometer System (VIRS), Precipitation Radar (PR), and Lightning Imaging Sensor (LIS) provide a three dimensional view of the internal structure of deep convection not presently available from any geostationary satellite, and thereby yield an unprecedented opportunity for evaluation of the OW diagnostic products. The coupling of lightning and rainfall observations helps to better understand the relationship between lightning and precipitation and the often-pronounced differences between maritime and continental cumulonimbus clouds.

A schematic illustration of the scanning geometry among the VIRS and PR instruments is shown in Figure 4. The VIRS instrument is a cross track scanning radiometer measuring scene radiance in five-channels and is similar to the Advanced Very High Resolution Radiometer

(AVHRR) aboard a National Oceanic and Atmospheric Administration (NOAA) spacecraft (Kummerow et al., 1998). The track width during the period of the intercomparisons was approximately 820 km wide. The footprint resolution slightly exceeds 4 km at nadir and increases toward the swath edges. The visible and infrared channels were used in the intercomparisons to link observed convective events to the PR data and to the three geosynchronous satellite-based detection algorithms.

An integrated perspective of continental convection points to the central role of the updraft in affecting aviation hazard. Physical bases for correlated relationships between updraft and turbulence intensity (Pinsky and Khain, 2002), updraft and icing/hail (Williams, 2001), and updraft and lightning activity (Williams, 1985; Baker et al., 1995; Boccippio, 2001) are now reasonably well established. Unfortunately, despite its central role, the updraft remains an elusive variable, even over continents where Doppler radar measurements are numerous. The vertical profile of radar reflectivity, a far more accessible internal observation, is often used as a surrogate for updraft (Williams et al., 1992; Petersen and Rutledge, 2001; Ushio et al., 2005; Cecil et al., 2005). This practice is continued in the present context.

The PR instrument is capable of obtaining three-dimensional information of precipitation over the land and oceans. The swath width of the radar is approximately 247 km with a horizontal resolution slightly more than 4 km at nadir and the vertical resolution is 0.25 km. The observable range of the radar extends from the near surface to a 15 km altitude. The normalSample product with no attenuation correction was used in the analyses. Of great importance to these studies is the reflectivity observed at higher altitudes (above the freezing level and throughout the so-called mixed phase region), which is the weakly attenuated portion of the cloud. The vertical resolution of the radar is excellent for documenting individual cumulonimbus clouds, but the horizontal resolution is less than ideal given that the diameters of reflectivity cores within such clouds are normally less than 4 km.

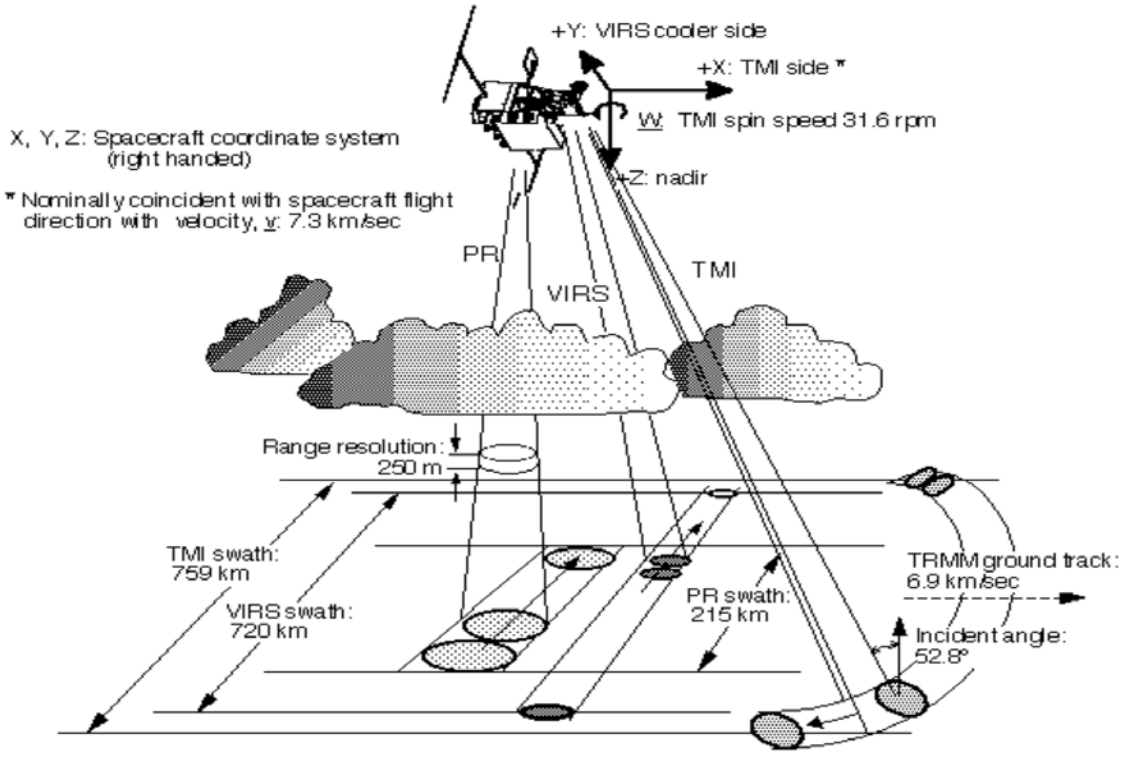

Figure 4. Schematic of the low earth orbiting TRMM satellite illustrating the scanning geometry of the Precipitation Radar (PR), Visible and Infrared Radiometer System (VIRS), and TRMM Microwave Imager (TMI). The Lightning Imaging Sensor (LIS) is not shown. From Kummerow et al. (1998).

The LIS (not shown in Figure 4) is an optical imager (Christian et al., 2003) that searches for transient pulses (intracloud and cloud-to-ground lightning) that rise above the radiance of the background scene. The optical detector has individual pixel resolutions from 3-6 km and a total field of view of 550x550 km^2. The LIS, in its nominal 100-minute LEO, typically observes a point on the Earth's surface for approximately 90 seconds. The elemental LIS data are stored in a structure and grouped so that they correspond to physical features such as thunderstorms, flashes and strokes. The *Area* and *Flash* groups (Boccippio et al., 1998) were extracted from the LIS database and used in the intercomparisons in the present study. Areas represent regions that were observed to contain one or more flashes and correspond to individual thunderstorm cells. Flashes represent the location of observed pulses that are close to each other in space and time, i.e., the physical lightning flash.

Another TRMM product used during the third intercomparison is the rain type classification generated from the PR Qualitative algorithm (Awaka, 1998). The objectives of this algorithm are to detect the radar bright band, classify the rain type and to detect warm rain. Rain types are sorted into three categories: stratiform, convective, or 'other' and are used as an additional metric for characterizing deep convective clouds with potential hazard to aviation.

5. IMPORTANT TERMINOLOGY USED WITHIN STUDIES

Within the context of the following sections that describe each intercomparison study, we define a *cumulonimbus cloud* as a dense and vertically developed cloud that does not contain lightning and a *thundercloud* as a cumulonimbus cloud accompanied by lightning. *Hazardous cell* and *hazardous convection* both refer to cumulonimbus clouds that pose a potential hazard to aviation. In the second and third intercomparisons, these terms are defined further by verifying in the TRMM data that the cell contained a single or combined signature of lightning, radar reflectivity $\geq$30 dBZ at 5 km altitude and convective rain. All references to *cell*, *convective cell*, *deep convection*, and *deep convective cloud* represent a vertically developed cloud identified in the TRMM and geostationary satellite based products that are potentially hazardous under the criteria mentioned above.

6. INTERCOMPARISON STUDIES

The domains under study in each of the three intercomparisons varied due to seasonal changes in the occurrence of deep convection. The first comparison took place on 10 June 2002 during the late morning to mid-afternoon hours local time when the TRMM satellite passed over the Caribbean, Gulf of Mexico, and south-central United States. The 10 June date was selected on short notice when deep oceanic and continental air mass thunderstorms were expected in the area. The test domain (15°-35° N latitude and 75°-105° W longitude) is shown in blue in Figure 5.

Due to the limited number of cells (32) analyzed in the first intercomparison, a longer period of study and a larger domain were chosen for the second exercise. The comparison took place during the daylight hours from 26-31 March 2003. Two regions were evaluated. One area was centered over northwestern South America (10° N – 20° S, 50°–80° W) where diurnal air mass thunderstorms were expected to be numerous. The other area was in the central Pacific Ocean (0°–20° N, 120°–150° W) covering a portion of the ITCZ where maritime convection was expected to be prevalent. The two regions of interest are shown in Figure 5 as yellow rectangles. The analysis times were restricted to daylight hours because at that time the NRL CC was unable to classify clouds at night.

A third intercomparison was planned to analyze additional maritime cells and to evaluate the capabilities and readiness of the individual diagnostic algorithms in another climatological region. This intercomparison was conducted over a much larger area in the western Pacific Ocean (35° S – 35° N, 120°–180° E). This area was chosen to capture several types of convection such as cold frontal systems in the central Pacific, tropical cyclone development within the ITCZ, and summer convection over Australia and Indonesia. Figure 5 illustrates the substantially larger domain size in the final intercomparison (red rectangle). Beginning on 4 February 2004, the OW algorithms were run daily, day and night, at three-hour intervals beginning at 02:25 UTC to coincide with the full disc scans of the GOES-9 satellite. A nighttime classifier was developed by NRL prior to the analysis, and the spatial resolution of the GCD product was increased to 4 km to be in agreement with the other diagnostic products.

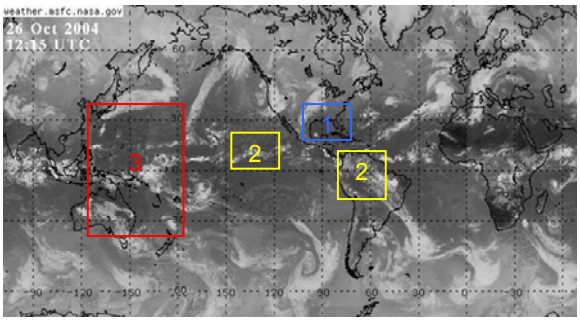

Figure 5. Global infrared imagery with each intercomparison region of interest outlined. The first, second, and third intercomparison areas studied are shown as a blue, yellow, and red rectangle, respectively. Global satellite imagery was acquired from the NASA Global Hydrology and Climate Center website, weather.msfc.nasa.gov.

In each intercomparison, all OW products and TRMM data were mapped to a common 4 km grid to assure proper spatial alignment.

6.1 First Intercomparison: 10 June 2002

A total of 32 convective cells were identified in three TRMM orbits that intersected the Gulf of Mexico region during the late morning and early afternoon hours. In this intercomparison, we define a match as any cell observed in the TRMM and geo-satellite based products where the two data sources were coincident within a 20-minute time window. Cells were selected based on a visual inspection of the VIRS data to identify any large cloudy region (area >700 km^2) with high reflectance (radiance ≥18,000 mW cm^{-2} μm^{-1} sr^{-1}) and a low cloud top temperature (≤230° K). The convective cells were sorted into two categories, as thunderclouds confirmed by the LIS or as cumulonimbus clouds not containing lightning. The OW products were then studied to determine their ability to detect both types of cells. The objective of the product evaluation was to determine how each algorithm performs in detecting thunderclouds, a known hazard to aviation, and deep cumulonimbus clouds that are believed to be hazardous, but at a level that is currently unknown.

Of the 32 convective cells identified, 16 were categorized as thunderclouds and 16 as more benign cumulonimbus clouds. The OW algorithms were each scored by noting whether or not any detection matched the cloudy area for the cell of interest. Due to temporal differences, the detection signatures are not expected to exactly overlap the corresponding TRMM features, so detection sizes were not evaluated. While the algorithms do not distinguish between cells on the basis of lightning they do identify the location of convective features. For the CTOP product, convection is identified as cloud tops that meet or exceed 40,000 feet. The CC product associates convection with the cumulonimbus or cirrostratus cloud that frequently accompanies deep convection. For the GCD product, satellite channel differences (water vapor channel - infrared channel) ≥–1° C coupled with a LI less than or equal to 1° C indicates deep convection.

Probability of Detection (POD) performances for each algorithm are shown in Table 1. The POD for each category type is the ratio of the number of thunderclouds (cumulonimbus clouds) detected as convection by the algorithm to the total number of thunderclouds (cumulonimbus clouds) verified by TRMM. The performance statistics of the CTOP algorithm at lower height thresholds are also provided in the table. The CC and GCD algorithms were able to detect greater than 85% of both cloud types while the CTOP algorithm performance was substantially lower, detecting only 38% and 56% of the thunderclouds and cumulonimbus clouds, respectively. The cloud heights of all the convective cells exceeded 30,000 feet, suggesting that the CTOP product would have benefited through use of a lower threshold setting. Due to the limited sophistication of the product evaluation and utilization of the TRMM data in this study, the false alarm ratio (FAR) was not computed.

While the TRMM radar data provide a means of observing the internal structure of a convective cell, this information was not used as a metric for categorizing cloud types in this intercomparison. However, these data were useful for generating vertical reflectivity profiles for 17 of the cells located in the narrow PR swaths and determining any characteristic differences in structure between the seven thunderclouds and ten deep convective clouds. Profiles were created by obtaining the maximum reflectivity value within a 14 km radius from the cloud center at each 250 m interval from near surface up to the 15 km altitude. Maximum reflectivity profiles for a thundercloud and cumulonimbus cloud observed in the Gulf of Mexico are shown in Figure 6. The thundercloud profile shows higher reflectivity values extending to higher altitudes in the cloud suggesting a vigorous updraft, whereas the highest reflectivity values within the cumulonimbus cloud are limited to the lower altitudes of the cloud indicating weaker updrafts within the cloud. Similar features were observed in the other seven maritime cloud profiles.

Table 1. Probability of Detection (POD) and fraction correct (in parentheses) for three satellite diagnostic products applied to detection of two types of cloud categories, thunderclouds and cumulonimbus clouds without lightning, during the first satellite intercomparison on 10 June 2002.

Satellite Product	Probability of Detection (POD)	
	Thunderclouds	Cumulonimbus clouds
Cloud Classification (CC)	1.0 (16/16)	0.94 (15/16)
Global Convective Diagnostic (GCD)	0.88 (14/16)	0.94 (15/16)
Cloud Top Height (CTOP) ≥ 40 kft	0.38 (6/16)	0.56 (9/16)
Cloud Top Height ≥ 35 kft	0.69 (11/16)	0.81 (13/16)
Cloud Top Height ≥ 30 kft	1.0 (16/16)	1.0 (16/16)

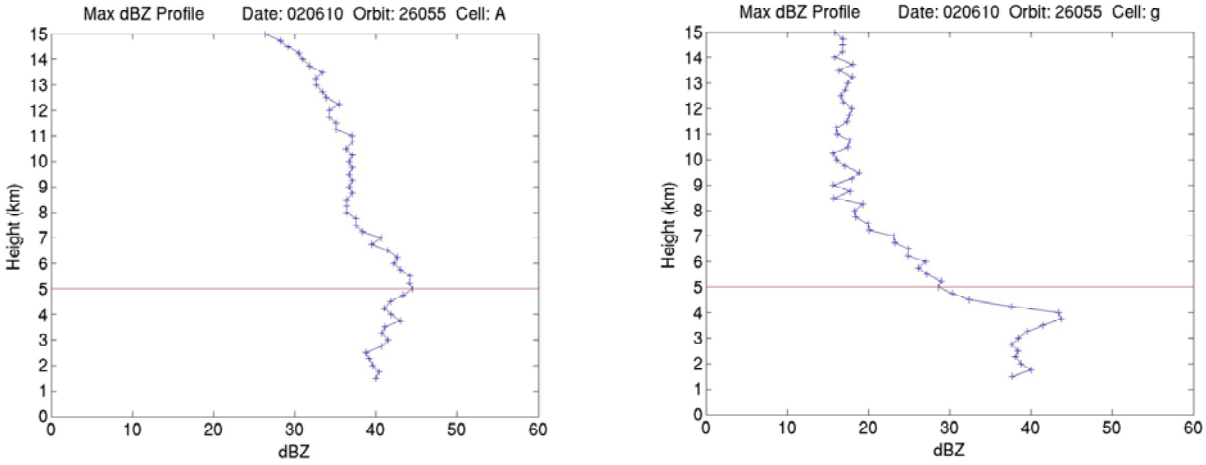

Figure 6. Maximum reflectivity profiles of convective cells observed by the TRMM PR over the Gulf of Mexico on 10 June 2002 for a thundercloud (left) and cumulonimbus cloud (right). The red horizontal line at the 5 km altitude in both plots represents the approximate freezing level in tropical regions.

The inherent difficulty that each diagnostic algorithm faces in determining the hazard level of a convective cell is that while the cloud type or cloud top height may be reasonably identified, none is able to decide how strong or turbulent the updraft velocities may be inside the cloud. Generally, as a cloud deepens, so does its maximum updraft speed (Williams, 1985) and peak lightning flash rate (Williams, 2001). The problem over the oceans is that deep convection is typically less energetic and less hazardous than that over land (LeMone and Zipser, 1980; Jorgensen and LeMone, 1989; Williams and Stanfill, 2002). Visible imagery of the TRMM overpass in a portion of the Western Atlantic and Gulf of Mexico in Figure 7 illustrates the difficulty in diagnosing hazardous oceanic convection. Based on general experience with convection over land, nearly all of the large, ominous cells suggest a real hazard to aviation, yet only four of them (shown with circles) contain lightning.

6.2 Second Intercomparison: 26-31 March 2003

The first comparison study was a 'catch as you can' style analysis yielding a small number of cells observed on one day. The second intercomparison was conducted over six days in late March 2003 and significantly extended the database of cases. Similar to the first comparison, the analysis was restricted to the daylight (local afternoon) hours, and a match refers to any cell identified in the TRMM and geo-satellite products at locations where the data were coincident within a 30-minute time window. Accounting for some data ingest problems with the OW products, analysis for the geo-satellite products was performed for a total of 14 Pacific and 8 South American TRMM overpasses. Unlike the first intercomparison, where the solar zenith angle of the GOES satellite was very small (i.e., the satellite was nearly overhead) some of the March cases occurred under conditions where the solar zenith angle was >82 degrees (as the day is transitioning to night). Since the darkening of the satellite imagery that

results can provide erroneous data leading to misclassifications of cloud type, the NRL algorithm was unable to perform cloud classifications under these circumstances.

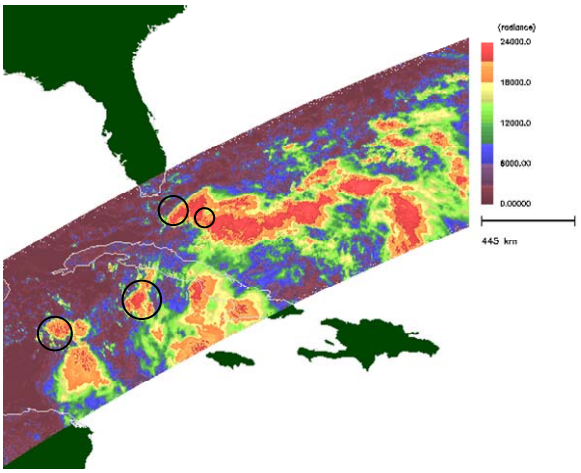

Figure 7. Visible imagery observed by TRMM taken at 15:22 UTC on 10 June 2002. Warmer colors denote colder and higher cloud top heights. Units for radiance are in $mWcm^{-2}\mu m^{-1}sr^{-1}$. While most regions of high cloud top appear hazardous to aviation, only four cells contain lightning (enclosed by circles). Image acquired from the TRMM Science Data and Information System (TSDIS) visualization software tool Orbit Viewer.

Because the goal of the OW PDT is to develop a real-time diagnosis of the locations of convective related hazards, the TRMM data are quite useful to differentiate between hazardous and non-hazardous cells and to evaluate the ability of each diagnostic to make such inferences. Consequently and in contrast with the first study, both radar and lightning observations were used to distinguish a hazardous cell from a non-hazardous cell. The TRMM LIS and PR data were examined for the presence of lightning or reflectivity values $\geq$30 dBZ at an altitude of 5 km. If one or both observations were made, the cell was considered hazardous and the OW diagnostic products were scored accordingly. A reflectivity criterion was chosen because significant reflectivity found in the mixed phase portion of a cloud is necessary for electrical charge separation and the formation of lightning (Ushio et al., 2005; Cecil et al., 2005) and could be used as a precursor to ensuing hazardous conditions to aviation. Such enhanced reflectivity also indicates that stronger vertical velocities exist within the cloud and could lead to more turbulent conditions near the updraft column. Outside the narrower PR swath of the TRMM orbit, the products were evaluated only if the cells contained lightning so as not to penalize the algorithms for making false detections where no underlying radar data were available. Cells were selected in a manner similar to the first intercomparison.

An example of the scoring methodology for two cells is shown in Figure 8 and the corresponding maximum reflectivity profiles are shown in Figure 9. Any cloud area was considered for analysis if it appeared to be convective within the VIRS visible imagery (top left image in Figure 8) and had low (i.e., cold) cloud top temperatures (IR image not shown). In this example, cell A, although spatially small, was characterized as hazardous because the reflectivity at 5 km was 45 dBZ (Figure 9a) and lightning was detected by the LIS. All three OW products correctly detected this cell. Cell B is significantly larger but was not considered hazardous because the reflectivity at 5 km was only 23 dBZ (Figure 9b) and no lightning was observed. The CC algorithm correctly did not classify this cloudy area in the deep convection class, whereas the GCD and CTOP algorithms both falsely indicate this cell to be hazardous by issuing detections and a maximum cloud top height of 42 kft, respectively.

All TRMM overpasses intersecting each domain of interest during the local afternoon hours were examined. One hundred seventeen hazardous cells were observed over land in the South American sector but only 20 hazardous cells over the ocean following the criteria stipulated above. OW product evaluation statistics were tabulated and categorized to show detection performance over land and ocean. The results are provided in Table 2. The scoring metrics are POD, False Alarm Ratio (FAR), and Critical Success Index (CSI). In this study, the POD is the ratio of the number of detected hazardous cells verified by TRMM (detections) to the total number of hazardous cells identified by TRMM. The FAR is the ratio of the number of detections not verified by TRMM (false alarms) to the total number of detections issued. The CSI is the ratio of the number of detections to the sum of detections, misses (failure to detect), and false alarms. The results in Table 2 show the CC having the best detection performance by detecting 98% and 100% of all land and ocean hazardous cells, respectively. The GCD also performed well at detecting greater than 75% of all the land and ocean cells while the CTOP algorithm showed the poorest performance by detecting 50% of the ocean cells using a cloud top height threshold of 40 kft. The FAR among the

algorithms was respectable at 14-17% for all land cells but increased for the CC and GCD over the ocean. With respect to CSI, the CC outperformed the other algorithms for the land cells due to fewer missed detections, but there was no clear frontrunner for the ocean cells. Employing lower height thresholds in the CTOP algorithm such as 30 and 35 kft yield much higher POD rates and fewer missed detections, but with an undesirable increase in the FAR.

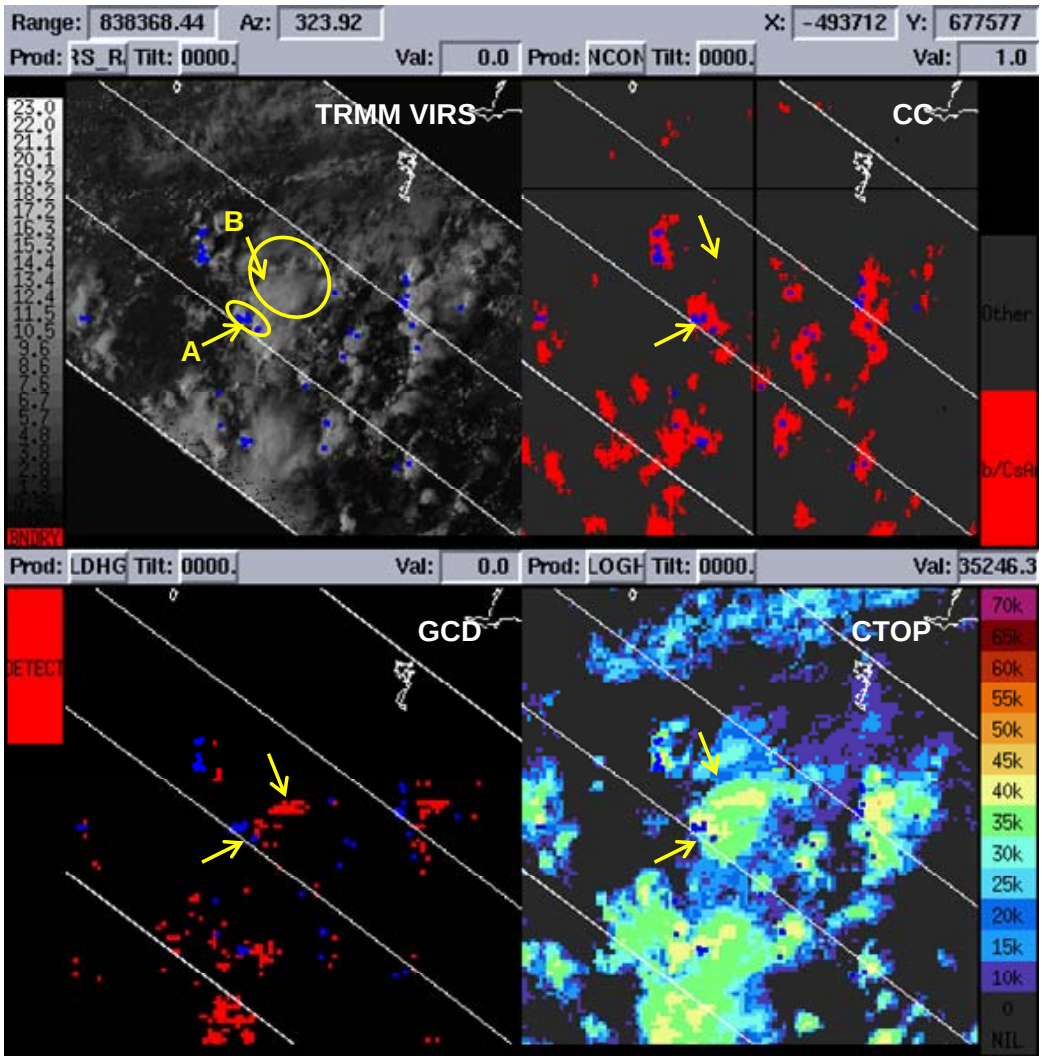

Figure 8. Four-panel analysis display showing TRMM visible imagery (upper left), CC detections of the cumulonimbus and cirrostratus associated with deep convection classes (upper right), GCD detections of satellite channel temperature differences ≥-1 ºC (lower left), and CTOP heights contoured in 5,000 ft intervals (lower right). The blue dots represent lightning flashes observed by LIS. The two parallel outer and inner lines represent the VIRS and PR swath edges, respectively. Two cells of interest are denoted as A and B, denoted by yellow ovals in upper left panel.

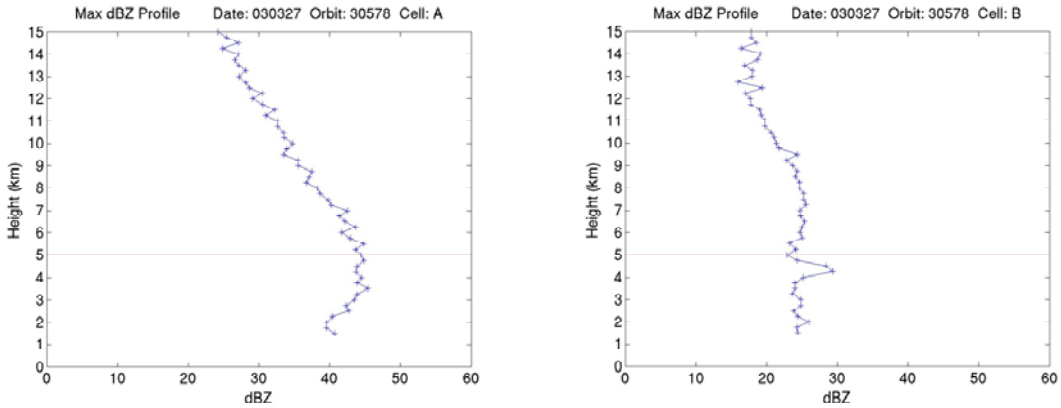

Figure 9. Maximum reflectivity profiles of two convective cells deemed to be hazardous (left) and non-hazardous (right) based on the criterion that the cell must contain lightning and/or measure reflectivity ≥30 dBZ at the 5 km altitude (red horizontal line). The profile on the left (refer to cell A in Figure 8) meets the reflectivity criterion (45 dBZ) and has lightning associated with it. The profile on the right (refer to cell B in Figure 8) does not contain lightning and has weak reflectivity at 5 km (23 dBZ).

Table 2. Detection performance statistics for the three satellite products during the second intercomparison. Performance results are separated between land (top) and ocean (bottom). The scoring metrics from left to right are as follows: Hits (number correct), Misses (failure to detect), False Alarms (incorrect detections), Bad (product not available), Detect (Hits + False Alarms), Probability of Detection (POD), False Alarm Ratio (FAR) and Critical Success Index (CSI).

South American Sector (117 Hazardous Cells over Land)								
Product	**Hits**	**Misses**	**False Alarms**	**Bad**	**Detect**	**POD**	**FAR**	**CSI**
CC	102	2	17	13	119	0.98	0.14	0.84
GCD	89	28	16	0	105	0.76	0.15	0.67
CTOP ≥ 40 kft	88	28	18	1	106	0.76	0.17	0.66
CTOP ≥ 35 kft	110	6	21	1	131	0.95	0.16	0.80
CTOP ≥ 30 kft	112	4	21	1	133	0.97	0.16	0.82
Pacific Sector (20 Hazardous Cells over Ocean)								
Product	**Hits**	**Misses**	**False Alarms**	**Bad**	**Detect**	**POD**	**FAR**	**CSI**
CC	20	0	17	0	37	1.00	0.46	0.54
GCD	16	4	7	0	23	0.80	0.30	0.59
CTOP ≥ 40 kft	8	8	0	4	8	0.50	0.00	0.50
CTOP ≥ 35 kft	15	1	8	4	23	0.94	0.35	0.63
CTOP ≥ 30 kft	16	0	15	4	31	1.00	0.48	0.52

Despite the small number of hazardous cells (20) observed over the oceanic domain, results from this study have yielded some significant results. While performance differences exist among the OW algorithms, each has shown a similar skill at identifying convection over land and ocean. However, the outstanding result of this study is that all algorithms tend to overestimate the presence of (presumed hazardous) maritime convection resulting in higher FARs. Finally, the maximum reflectivity profiles indicate the oceanic cells are weakly developed in the mixed phase region of the cloud, despite the presence of high (>10 km) cloud tops.

6.3 Third Intercomparison: 4 February – 31 March 2004

Unlike the first two intercomparisons scheduled to coincide with the availability of TRMM data over the target area when convective systems were expected, the spatial area chosen

for the third intercomparison is large enough to coincide with several TRMM overpasses each day. Products were generated at 3-hour intervals beginning at 02:25 UTC each day to coincide with the update rate of the GOES-9 full disk satellite scans and to accommodate potential limitations in processing power, disk space storage, and latencies in real-time data acquisition. In contrast with the first two intercomparisons, all OW products were evaluated both during the day and at night due to NRL's recent development of a nighttime CC algorithm. The spatial resolution of the GCD product was also improved from 10 km to 4 km.

Special consideration was given to the temporal matching of the TRMM and geo-satellite product data sets given the very large domain of the test. By knowing the start time and the elapsed time required to complete the full disk images at the selected time intervals, it was possible to estimate the time of day for a given cell of interest in the geostationary data if the latitudinal location was known. The OW product data were evaluated in regions where the approximate time of day matched the time-registered TRMM data to within 15 minutes. All other regions within the data grids that were not time coincident were excluded from evaluation.

The scoring methodology was similar to that used in the second intercomparison, i.e., estimating the degree of hazard of each cell using TRMM LIS and PR data for verification. However, a third criterion for hazard was added, namely the NASA method for classifying convective rain (termed the "TRMM Qualitative product"). This rain product employs a vertical profile and horizontal pattern method (Steiner et al., 1995) to distinguish between stratiform and convective rain systems. It was decided that a small region (<10 pixels) classified as convective rain detections alone would not be classified as hazardous unless it was accompanied by lightning or significant upper level reflectivity. Convective rain detections ≥10 pixels were classified as hazardous cells.

Furthermore, the convection evaluated by each diagnostic product was sorted independently into two convective regimes, 'maritime' or 'continental', distinguished on the basis of fractional area of coverage of radar reflectivity ≥20 dBZ at the 5 km altitude. This decision was based on earlier ground-based radar studies in the tropics (Williams et al., 1992) showing substantial differences in the fractional area of radar echo coverage between true continental and maritime regimes. The fractional area is the ratio of the number of pixels exceeding 20 dBZ at the 5 km altitude to the total number of pixels within a bounding box that has a width and length equal to the PR swath width (~247 km) and is centered on the cell of interest. As shown by Williams et al. (1992), a cell exhibits 'maritime' characteristics (large cloudy area with high cloud tops and little or no lightning) if the fractional area with radar reflectivity exceeding some threshold is large. A histogram distribution of the fractional areas computed for all hazardous cells identified in the TRMM radar data (583) is provided in Figure 10. It's clear that a high percentage of cases exhibit small fractional areas (<10%) and by inference, 'continental' characteristics. Several cell centers located near the PR swath edges did not have as large an area from which to collect reflectivity data. The fractional area computation for these cells may yield results not representative of the actual storm status but the occurrence was low and the overall impact on the analysis negligible.

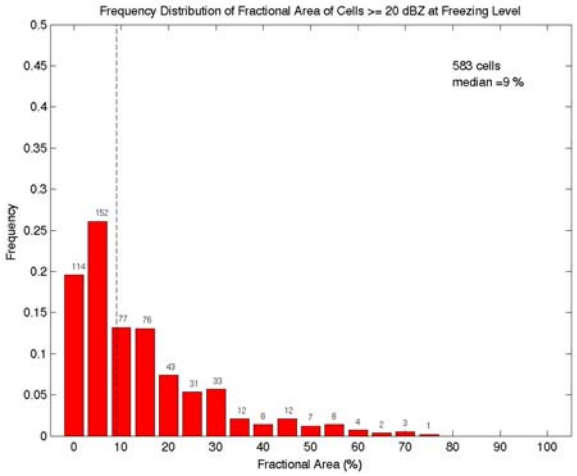

Figure 10. Frequency distribution histogram of the fractional area of radar reflectivity ≥20 dBZ at the approximate freezing level (5 km) for all hazardous cells within the TRMM PR swath. The dashed vertical line represents the median of the sample (9%) and was chosen to distinguish 'continental' (left of line) from 'maritime' (right of line) style convective cells.

An illustration of the analysis display used for identifying common convective features in the various satellite data sets is provided in Figure 11. The evaluation was restricted to cells located within the PR swath (denoted as the region inside the two parallel lines) and those cells that contained lightning located outside the radar swath and inside the VIRS swath. A composite of the TRMM products indicating which cells contain hazardous signatures is shown in the bottom

middle panel. The fractional area used to distinguish between 'continental' and 'maritime' style cells binned at 10% intervals is shown in the bottom right panel. A dividing line of 9% was selected as the value that roughly split the total population equally.

Within the two-month period studied, 649 cells were deemed hazardous following criteria discussed above. Performance statistics of the OW products were compiled and are illustrated in Figure 12. All cells containing lightning and located outside the PR swath (66) were included in the evaluation results and is the reason for the increase in the hazardous cell count not included in the fractional area distribution plot (Figure 10). The CC algorithm performed best overall in terms of detection with a POD of 78%. However, this algorithm was the most aggressive in over-detecting the presence of hazardous convection with a FAR of 34%. Whether the fact that the CC algorithm uses GOES-8 and GOES-10 training data and is being applied to GOES-9 imagery contributes to this output is unknown. The CTOP algorithm (using a 40 kft threshold) performed moderately well with a 63% POD and a 21% FAR. Again, similar to the previous studies, lowering the cloud top height threshold from 40,000 ft to 30,000 ft would have raised the POD by 28% with only a modest increase (7%) in the FAR (not shown in Figure 12). The GCD performed the least well and was the most conservative in the number of detections issued (more than 50% fewer detections than CC and CTOP). Less detection issued led to the lowest FAR (12%) but also resulted in a low POD (37%). The GCD results indicate that the temperature difference threshold and/or the stability index filter were too stringent. In regards to overall performance, the CSI of the CC and CTOP algorithms were similar at 55% and nearly a 20% improvement over the GCD.

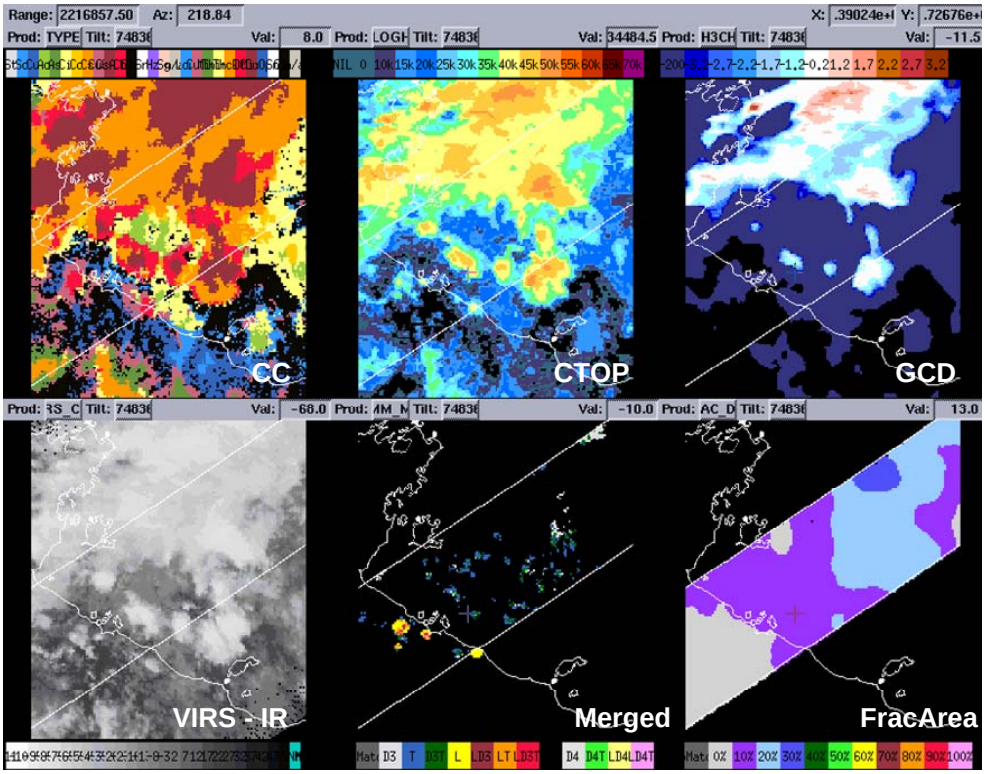

Figure 11. Illustration of an analysis display used to evaluate the convection diagnostic products (top images) with the TRMM product data (bottom images) observed in the Gulf of Carpentaria (upper right of each image) and northern Australia (lower and left portion of each image) on March 18, 2004 at 05:38 UTC. The TRMM Merged data (bottom middle image) were used to record single or combined observations of lightning (L), reflectivity values above 30 (D3) and 40 (D4) dBZ at 5 km altitude or convective rain (T) and the fractional area of radar reflectivity ≥20 dBZ (bottom right image) were used to distinguish between a 'maritime' or 'continental' regime.

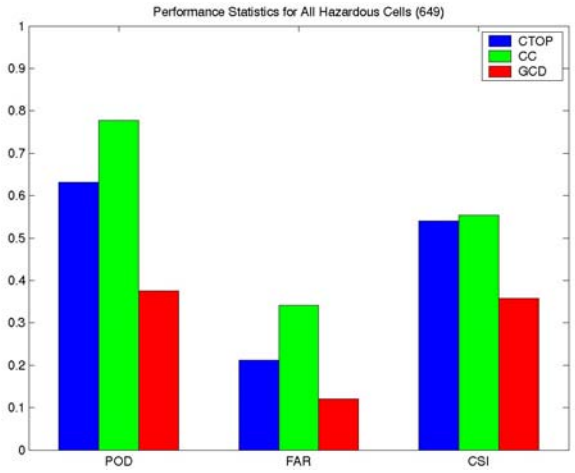

Figure 12. Histogram of the performance statistics for the CTOP (blue), CC (green), and GCD (red) algorithms in the third intercomparison. A total of 649 cells were identified in the TRMM data as possibly hazardous. The scoring metrics are defined as the Probability of Detection (POD), False Alarm Ratio (FAR), and Critical Success Index (CSI).

The scoring statistics were broken down further into each algorithm's ability to detect hazardous cells over the ocean or land, during the day or at night, and whether they exhibited 'maritime' or 'continental' characteristics based on the fractional area test. Results for each category are shown in Figure 13. Despite the fact that 79% of the hazardous cells were observed over the ocean, due in part to the considerably large oceanic region being studied (Figure 5), there is no discernable difference in performance at identifying the cells (POD) over land from those over the ocean. This result is consistent with the second intercomparison. When comparing individual performance, the CTOP (using a 40 kft threshold) and CC algorithms show marginally better performance with the cells over land than over the ocean (8% CSI increase) and both show a similar trend in overestimating the convection hazard over the ocean than over land (8% and 11% increase in FAR, respectively). Further review of the CTOP detections over the ocean show that many of the cloud top heights of the missed cells were in the 34–38 kft range. The GCD algorithm showed little difference in performance for land and ocean cells. However, there was more variability in the temperature channel differences for the missed cells over ocean than over land.

For both land and ocean cells, the statistics also reveal that all algorithms perform markedly better at identifying the cells classified as 'maritime' (i.e., cells that are accompanied with a large well-developed cloud mass with a significant spatial distribution of reflectivities in the mixed phase region) over cells classified as 'continental' (i.e., cells with small fractional area). Similar performance differences were noted between the 'continental' and 'maritime' style cells when looking further into the subset of cases located specifically over the ocean. Analysis of the hazardous cells not detected by the algorithms reveals significantly more variability in the detection values among all the algorithms for cells classified as 'continental'. This observation coupled with the poorer performance in measured FAR could be due to a combination of factors: (1) the time allowance (15 minutes) used during the TRMM and GOES grid matching where the smaller cells may have rapidly developed (decayed) to (from) a hazardous level as viewed by the TRMM satellite but not in the GOES satellite-based products, and (2) the reflectivity sampling of the PR (with its less-than-ideal ~4 km horizontal resolution) did not capture the small reflectivity cores, hence reducing the number of 'hazardous' cells identified and increasing the opportunity for false alarms.

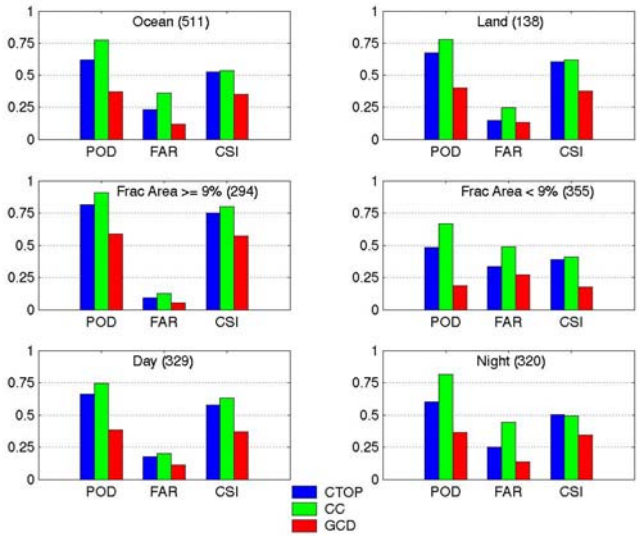

Figure 13. Performance statistics among the three algorithms in their ability to detect hazardous cells in the third intercomparison distinguished on whether the cell was located over the ocean or land (top histograms), exhibited large and small fractional area of radar reflectivity ≥20 dBZ at 5km altitude (middle histograms), and observed during the day or at night (bottom histograms). The scoring metrics are defined as the Probability of Detection (POD), False Alarm Ratio (FAR), and Critical Success Index (CSI).

Regarding comparison of detection performance between the day and nighttime cells, the CTOP and GCD algorithms perform similarly with respect to each other with an equal distribution in the variability of detections among the missed cells. The CTOP CSI was 7% higher for the daytime cells. The CC algorithm shows an improved detection rate, a distinct increase in the FAR, and a 14% reduction in CSI for nighttime cells. The increase in CC POD (7%) and FAR (24%) is likely an artifact of the aggressive algorithm behavior at night and can probably be attributed to the loss of the satellite visible channel information. Lack of any higher resolution data (visible channel is 1 km vs. 4 km for infrared channels) and use of larger sample boxes can lead to misclassifications at night. The bias toward deep convection needs further study to quantify the difference in performance.

Figure 14 contains frequency distribution plots of the output values issued by each algorithm for all hazardous cells identified. The dashed vertical lines in the CTOP and GCD plots represent the current algorithm threshold used to diagnose deep convection. All values of cloud top height (top plot) to the right (left) of the vertical line denote algorithm hits (misses). The abundance of missed detections in the 30-39 kft range suggests the need to lower the threshold to catch this subset of cases. The three dashed lines in the CC plot (middle) represent correct identifications of cloud type for deep convection. The two (one) on the left (right) represent the deep convection cloud categories in the daytime (nighttime) classifier. The misclassification of the daytime cells all seem to fall into cloud categories that have some vertical development (i.e., Cu – cumulus and Cg – cumulus congestus) or reside at high altitudes (i.e., Ci – cirrus and Cs – cirrostratus). Note that the algorithm does not misdiagnose low or mid-level cloud types. Among the few cells missed at night, most were identified in the mixed (Mx) type category (thin high clouds over low clouds), which may be due to the similarity in texture and/or pixel value variability within a given sample (between DC and Mx types). In the GCD detection plot (bottom plot in Figure 14), satellite channel temperature differences to the right (left) of the dashed vertical line correspond to hits (misses). The extension of temperature differences to –25 °C is not well understood at present.

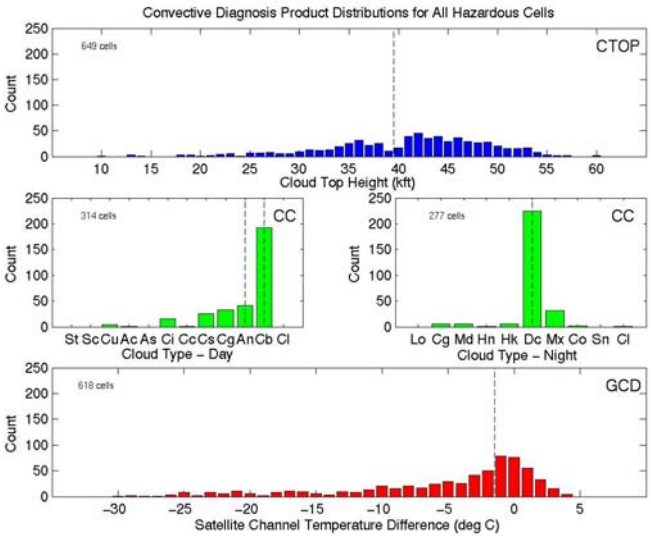

Figure 14. Distribution histograms of the detections issued by the CTOP (top), CC for daytime (middle left) and nighttime (middle right), and GCD (bottom) algorithms for all hazardous cells identified in the third intercomparison. Detections to the right of the dashed vertical lines in the CTOP and GCD plots represent correct diagnosis of deep, potentially hazardous convection. The dashed lines in both CC plots represent correct cloud category identifications of hazardous convection. The An, Cb, and DC cloud categories correspond to cirrostratus cloud associated with deep convection, cumulonimbus cloud, and deep convection at night, respectively. Fewer cells were evaluated for the CC and GCD products due to algorithm data availability.

Performance statistics among the three algorithm products in their ability to detect the strongest hazardous cells, namely, those that contained lightning (105), over both land and ocean combined, are presented in Table 3. The Probability of Missed (POM) detections is included in the table and represents the ratio of the number of thunderstorms not detected to the total number of thunderstorms identified by the TRMM LIS (i.e., 1-POD). FAR and CSI do not apply here because the algorithms should not be penalized for identifying deep, potentially hazardous convection that do not contain lightning. The CC algorithm obtained the highest POD (84%) overall followed by the CTOP (67%) and the GCD (43%). These statistics are a 4-7% improvement over the detection rate of the hazardous cells that exhibited single or combined signature of reflectivity, convective rain or lightning. It is particularly noteworthy that the largest values for POD are achieved when lightning alone is used as a

criterion for 'hazardous cell'. Among the thunderstorms missed by the algorithms, more than 50% were located outside the PR swath where no reflectivity information was available for further study. However, consistent with the product value distribution charts shown for all hazardous cells (Figure 14), the product values were not that far off from current algorithm thresholds for this subset of cells.

Table 3. Performance statistics among the algorithms in their ability to identify the strongest hazardous cells, i.e., those cells that contained lightning, observed over land and ocean (105) during the third intercomparison. The scoring metrics from left to right are as follows: Hits (number correct), Misses (failure to detect), Bad (product not available), Probability of Detection (POD), and Probability of Missed (POM) detections.

Hazardous Cells Containing Lightning (105)					
Product	**Hits**	**Misses**	**Bad**	**POD**	**POM**
CC	80	15	10	0.84	0.16
GCD	43	56	6	0.43	0.57
CTOP ≥ 40 kft	70	35	0	0.67	0.33
CTOP ≥ 35 kft	86	19	0	0.82	0.18
CTOP ≥ 30 kft	97	8	0	0.92	0.08

The mean maximum reflectivity profiles (defined in Section 6.1, paragraph 4) for various subsets of categories were also studied. Figure 15 contains a plot of the mean profiles for all lightning-containing cells identified by the LIS subdivided into classes of ocean-continental (blue), ocean-maritime (green), land-continental (red), and land-maritime (yellow). As expected, the mean land profiles are stronger than the oceanic profiles (Petersen et al., 2001; Cecil et al., 2005). Of greater importance is the fact that the maritime profiles are stronger than the continental profiles, especially for the cells over the ocean. This comparison is consistent with the differences observed between the mean flash rate of the maritime (1.85 flash/minute) and continental cells (1.38 flashes/minute). The mean profile of all cells presumed to be hazardous over the ocean (following the criteria described earlier) was then compared and are shown in Figure 16. The 'maritime' profile is again stronger at all altitudes especially from the near surface up to the 6 km altitude.

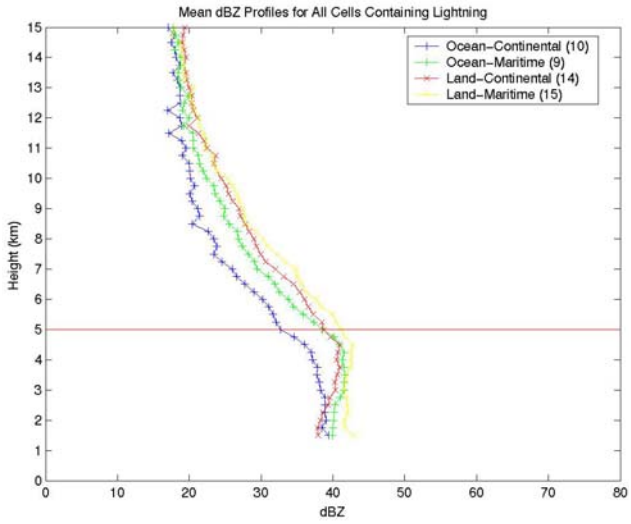

Figure 15. Profiles of mean reflectivity vs. height for all the cells that contained lightning distinguished on the basis of the fractional area test. Profiles are subdivided into categories of cells over the ocean that exhibited 'continental' (blue) or 'maritime' (green) characteristics and over land (red and yellow, respectively).

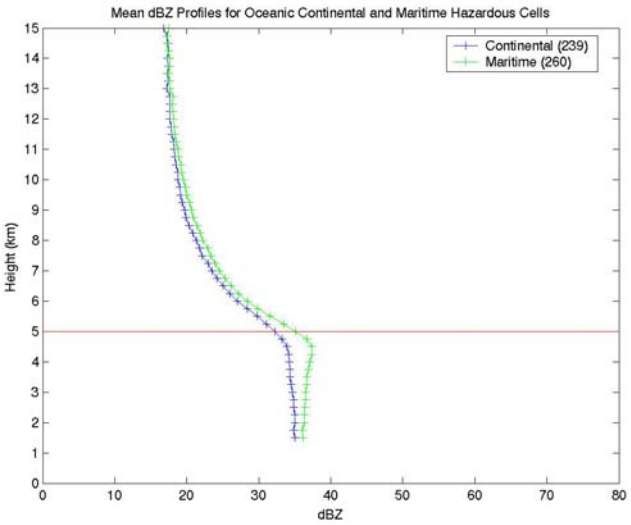

Figure 16. Profiles of mean reflectivity vs. height among all the oceanic cells presumed hazardous and distinguished on the basis of the fractional area test. Note the 'maritime' cells exhibited the strongest mean profile, particularly below 6 km.

7. DISCUSSION AND INTERPRETATION

Some consistent results emerge across the three satellite intercomparisons. The good news in the operational context is that the majority of TRMM-verified hazardous cells are correctly identified by the diagnostic algorithms. (This is to say that the POD values in Tables 1, 2 and 3 and

Figures 12 and 13 can exceed 90% when observed lightning is used as the criterion for 'hazardous' status). One cannot expect perfect algorithm detection in the presence of both imperfect algorithms and imperfect verification. The horizontal resolution of the TRMM PR can smear narrow reflectivity cores, and the time skew between the geostationary satellite products and the TRMM observations can allow storm evolution to negatively impact the verification process.

The not-so-good news in the operational context is that a substantial number of convective cells not verified as thunderstorms, or not deemed hazardous by other criteria, can masquerade (or 'false alarm') as hazardous cells. (This is to say that the FAR values are substantial in the cases that comprise Tables 1 and 2 and Figures 12 and 13, and occasionally exceed 40%). This latter result is also manifest at a larger scale in comparisons of global maps of thunderstorms and cumulonimbus clouds not containing lightning. The oceanic regions are relatively richer in the latter category than the former (see also Williams, 2005).

This unfavorable result exposes a fundamental limitation in the use of satellite visible and IR observations (in isolation) for identifying hazardous weather. The origin of this problem has been traced to a simple cause: a large number of oceanic cumulonimbus clouds attain high altitude but lack a strong updraft (and attendant radar reflectivity aloft and associated lightning activity). This result stands in marked contrast with the large body of evidence for continental convection, showing that clouds attaining tropopause heights are almost invariably producing lightning and presenting a legitimate hazard to aviation. In extreme continental situations, the tendency for severe weather hazard over land to increase with cloud height is well established (Darrah, 1978). Furthermore, the tendency for lightning flash rate to increase strongly with cloud height is also well established (Williams, 1985; 2001; Ushio et al., 2005). This situation invites another look at the differences between continental and oceanic convection for further understanding. Given the restricted latitude limits for verification by the TRMM satellite (+/- 35°), most of the discussion herein pertains to lower latitudes, where deep convection attains the greatest altitude in general.

A useful starting point for this discussion is a consideration of land-ocean contrasts in relevant cloud/thermodynamic parameters in Table 4. These rough estimates are extracted from the literature on Convective Available Potential Energy (CAPE) (Williams and Renno, 1993; Lucas et al., 1994; Williams and Stanfill, 2002; Zipser, 2003), level of neutral buoyancy (LNB) (Williams and Renno, 1993), cloud heights (Hendon and Woodberry, 1993; Anyamba et al., 2000; this study), updraft speed (Zipser et al., 1980; Williams and Stanfill, 2002), updraft width (Williams and Stanfill, 2002), cloud base height (Lucas et al., 1994; Betts, 1997; Williams and Stanfill, 2002; Williams et al., 2005) and concentration of cloud condensation nuclei (CCN) (Williams et al., 2002).

Table 4. Rough estimates of the approximate contrast in relevant cloud/thermodynamic parameters between land and ocean convection. CAPE, LNB, and CCN refer to Convective Available Potential Energy, Level of Neutral Buoyancy, and Cloud Condensation Nuclei, respectively.

Land-Ocean Contrast in Relevant Parameters	
Quantity	**Approximate Land-Ocean Contrast**
CAPE	10 %
LNB	10 %
Cloud Heights	10 %
Updraft Speeds	x 2-5
Updraft Widths	x 2
Cloud Base Height	x 2 or more
CCN	x 10

The traditional explanation for the contrast in observed updraft speed between land and ocean is based on parcel theory and CAPE. The ocean surface is mobile and is characterized by large heat capacity, both of which serve to suppress surface temperature rise by incident sunlight and the strong destabilization of surface air parcels. However, more recent scrutiny has shown that the contrast in CAPE between land and ocean is not adequate to explain the contrast in updraft speeds (Williams and Renno, 1993; Lucas et al., 1994; Williams and Stanfill, 2002; Zipser, 2003). The maximum wet bulb potential temperatures are larger over land, but so are the temperatures at mid-levels of the atmosphere (Williams and Renno, 1993). So both the temperature sounding and the wet bulb adiabats are displaced slightly leftward for the oceans, with relatively little change (Table 4) in the LNB, which is the parcel theory indicator of cloud top height. This is to say that the land and the ocean are "convectively adjusted" in some sense. On this basis, one does not expect large differences in cloud height between land and ocean, regardless of the contrast in updraft speed (Table 4).

Williams and Stanfill (2002) and Williams et al. (2005) have presented evidence that departures from parcel theory are essential in explaining the contrast in updraft speed between land and ocean. Larger rising parcels are expected with higher cloud base heights and thicker boundary layer reservoirs of unstable air (Williams et al., 2005). These larger parcels are more immune to mixing and more likely to attain ascent speeds in line with parcel theory predictions (Williams and Stanfill, 2002). Observational differences in both cloud base height and updraft width (Table 4) are substantial between land and ocean, and can account for the large contrast in updraft speed.

The aerosol hypothesis (Williams et al., 2002; Rosenfeld and Woodley, 2003; Khain et al., 2005) presents a different explanation for the contrast in updraft strength between land and ocean, based on the early formation of 'warm rain' and the consequent super adiabatic loading of the updraft parcel (Khain et al., 2005). This idea is not strongly supported by the vertical profiles of radar reflectivity in Figure 15 showing little tendency for stronger profiles at lower levels in the more maritime cases. More importantly, the aerosol hypothesis does not account for the systematic differences in updraft width between land and ocean (Williams and Stanfill (2002) and Table 4) that we link with differential departures from parcel theory.

The new comparative results over the oceans using fractional area as a parameter in the third satellite intercomparison (Figure 16) can likewise be interpreted in the context of a departure from parcel theory. Here it was shown that the vertical profiles of radar reflectivity were stronger, on average, in the cases exhibiting large fractional area. This finding ran contrary to our initial expectations concerning 'continental' and 'maritime' characteristics and our expectations based on parcel theory. Namely, the underlying ocean surface would experience stronger heating in the (less obscured) low fractional area case, with corresponding greater instability, stronger updraft, and stronger vertical reflectivity profile.

We do not expect a difference in cloud base height for the low and high fractional area cases, as they are both oceanic cases for which the surface relative humidity is close to 80%. But if departures from parcel theory are considered (noted initially in the Thunderstorm Project (1949) results), it can be expected that cases with low fractional area will be more susceptible to entrainment of drier environmental air (and subsequent dilution) than the high fractional area cases that are more likely surrounded with saturated air. We are not aware that comparisons of this kind have been previously undertaken.

The broad conclusion in considerations of both the observations in this study and the work documented in the literature is that departures from parcel theory are essential in accounting for the weak updrafts in deep oceanic clouds. An important caveat from an operational standpoint is the possibility that deep oceanic cumulonimbi without lightning and without enhanced radar reflectivity aloft will present a significant hazard to aviation.

8. CONCLUSIONS

Three different laboratories (NRL, NCAR, AWC) have each developed algorithms that use visible and infrared geostationary satellite information to diagnose deep convection that is possibly hazardous to aviation over oceans. These diagnoses have been verified with an independent data set from the NASA TRMM satellite for three intercomparison periods in the interval 2002-2005. Despite shortcomings in verification due to horizontal resolution in the TRMM PR sampling and modest (~15 min) time skew among the data sets, the algorithms have shown an ability to detect a large fraction of the most hazardous cells, those that contained lightning. However, each algorithm also has a tendency to overestimate the presence of hazardous oceanic convection, a situation one could improve through adjustments in thresholds for hazard.

Results from this study illustrate a fundamental limitation in using satellite visible and infrared information alone to make proper inferences about the internal characteristics of deep convective cells over the ocean, specifically the hazards associated with updraft strength and turbulence. Comparisons in the relevant thermodynamic parameters between land and ocean are discussed and do not help to explain the differences in updraft strength for clouds attaining similar cloud top heights from parcel theory alone. A fractional area test of the spatial reflectivity observed in the mixed phase region of the cloud was introduced in the third intercomparison to distinguish hazardous cells exhibiting 'maritime' and 'continental' characteristics. Contrary to our expectations and a departure from parcel theory, the vertical reflectivity structure within the maritime cells was stronger on average than in the continental cells. It is believed that entrainment of dry air and the subsequent erosion of the cloudy area is occurring in cells exhibiting low fractional area, whereas the

high fractional area cells are surrounded by saturated maritime air and hence protected.

9. ACKNOWLEDGEMENTS

This work was funded by the Aviation Weather Research Program (AWRP) of the Federal Aviation Administration (FAA). We thank Gloria Kulesa, Pete Kirchoffer and Warren Fellner for their support. The views expressed are those of the authors and do not necessarily represent the official policy or position of the FAA.

The TRMM visible, IR and radar data used for verification in these intercomparisons were provided by the Goddard Distributed Active Archive Center (DAAC) and with much assistance from the TRMM Science Data and Information System (TSDIS) helpdesk. Data from the TRMM Lightning Imaging Sensor were provided by the Global Hydrology Research Center (GHRC), NASA Marshall Space Flight Center (MSFC).

10. REFERENCES

Anyamba, E., E. Williams, J. Susskind, A. Fraser-Smith and M. Fullekrug, 2000: The Manifestation of the Madden-Julian Oscillation in Global Deep Convection and in Schumann Resonance Intensity, J. Atmos. Sci., 57, 1029-1044.

Awaka, J., T. Iguchi, and K. Okamato, 1998: Early Results on Rain Type Classification by the Tropical Rainfall Measuring Mission (TRMM) Precipitation Radar, Proc. 8th URSI Commission F Open Symp., Aveiro, Portugal, 143-146.

Baker, M.B., H.J. Christian and J. Latham, 1995: A Computational Study of the Relationships Linking Lightning Frequency and Other Thundercloud Parameters, Quart. J. Roy. Met. Soc., 121,1525-1548.

Betts, A.K., 1997: The Parameterization of Deep Convection. In Smith, R.K. (Ed.), *The Physics of Parameterization of Moist Atmospheric Convection*, Kluwer, Dordrecht, pp. 255-279.

Boccippio, D.J. et al., 1998: LIS/OTD Software Guide, Global Hydrology and Climate Center, NASA Marshall Space Flight Center.

Boccippio, D.J., 2001: Lightning Scaling Relations Revisited, J. Atmos. Sci., 59, 1086-1104.

Byers, H.R. and R.R. Braham, 1949: *The Thunderstorm*, U.S. Government Printing Office, Washington, D.C.

Cecil, D.J., S.J. Goodman, D.J. Boccippio, E.J. Zipser, and S.W. Nesbitt, 2005: Three Years of TRMM Precipitation Features. Part I: Radar, Radiometric, and Lightning Characteristics, *Mon. Wea. Rev.*, **133**, 543-566.

Christian, H.J., R.J. Blakeslee, D.J. Boccippio, W.L. Boeck, D.E. Buechler, K.T. Driscoll, S.J. Goodman, J.M. Hall, W.J. Koshak, D.M. Mach, and M.F. Stewart, 2003: Global Frequency and Distribution of Lightning as Observed from Space by the Optical Transient Detector, J. Geophys. Res., 108, 4005, doi: 10.1029/2002JD002347.

Darrah, R.P., 1978: On the Relationship of Severe Weather to Radar Tops, *Mon. Wea. Rev.*, **106**, 1332-1339.

Hendon H.H. and K. Woodberry, 1993: The Diurnal Cycle of Tropical Convection, J. Geophys. Res., 98, 16623-16637.

Herzegh, P.H., E.R. Williams, T.A. Lindholm, F.R. Mosher, C. Kessinger, R. Sharman, J.D. Hawkins, D.B. Johnson, 2002: Development of Automated Aviation Weather Products for Oceanic/Remote Regions: Scientific and Practical Challenges, Research Strategies, and First Steps, 10th Conference on Aviation, Range, and Aerospace Meteorology 13-16 May, 2002, Portland OR. Amer. Meteor. Soc., 57-60.

Jorgensen, D.P. and M.A. LeMone, 1989: Vertical Velocity Characteristics of Oceanic Convection, *J. Atmos. Sci.*, **46**, 621-640.

Khain, A., D. Rosenfeld and A. Pokrovsky, 2005: Aerosol Impact on the Dynamics and Microphysics of Deep Convective Clouds, Quart. J. Roy. Met. Soc., 131, 1-25.

Kummerow, C., W. Barnes, T. Kozu, J. Shiue, J. Simpson, 1998: The Tropical Rainfall Measuring Mission (TRMM) Sensor Package, *Journal of Atmospheric and Oceanic Technology*, **15**, 809-817.

LeMone, M.A. and E.J. Zipser, 1980: Cumulonimbus Vertical Velocity Events in GATE. Part 1: Diameter, Intensity and Mass Flux, *J. Atmos. Sci.*, **37**, 2444-2457.

Lucas, L., E.J. Zipser and M.A. LeMone, 1994: Convective Available Potential Energy in the Environment of Oceanic and Continental Clouds: Corrections and Comments, J. Atmos. Sci., 51m 3829-3830.

Mahoney, J., B. Brown, C. Mueller, and J. Hart, 2000: Convective Intercomparison Exercise: Baseline Statistical Results. Preprints, 9th Conference on Aviation, Range, and Aerospace Meteorology, Orlando, FL. Amer. Meteor. Soc. 403-408.

Martin, D.W., R. A. Kohrs, F. R. Mosher, C. M. Medaglia and C. Adamo, 2005: Over-Ocean Validation of the Global Convective

Diagnostic, Weather and Forecasting, (in review).
Miller, S**.,** T. Tsui, G. Blackburn, C. Kessinger, P. Herzegh, 2005: Technical Description of the Cloud Top Height (CTOP) Product, The first component of the Convective Diagnostic Oceanic (CDO) Product, Unpublished manuscript.
Mosher, F., 2002: Detection of Deep Convection Around the Globe, In Preprints, 10th Conference on Aviation, Range, and Aerospace Meteorology 13-16 May, 2002, Portland, OR. Amer. Meteor. Soc., 289-292.
Petersen, W.A., and S.A. Rutledge, 2001: Regional Variability in Tropical Convection: Observations from TRMM. J. Climate, 14, 3566-3586.
Pinsky, M. and A. Khain, 2002: Effects of In-cloud Nucleation and Turbulence on Drop Spectrum Formation in Cumulus Clouds, Q.J.R. Meteorol. Soc., **128**, 501-533.
Rosenfeld, D. and W.L. Woodley, 2003: Closing the 5-year Cycle: From Cloud Seeding to Space and Back to Climate Change through Precipitation Physics, Chapter 6 in "Cloud Systems, Hurricanes and Tropical Rainfall Measuring Mission (TRMM)", Ed., W.-K. Tao and R. Adler, Meteorol. Monogr., 51, 59-80.
Steiner, M., R.A. Houze Jr., and S.E. Yuter, 1995: Climatological Characterization of Three-Dimensional Storm Structure from Operational Radar and Rain Gauge Data, *J. Appl. Meteor.*, **34**, 1978-2007.
Tag, P.M., R.L. Bankert, and L.R. Brody, 2000: An AVHRR Multiple Cloud-Type Classification Package, *J. Appl. Meteor*., **39**, 125-134.
Takahashi, T., 1978: Electrical Properties of Oceanic Tropical Clouds at Ponape, Micronesia, *Mon. Wea. Review*, **106**,1598-1612.
Ushio, T., S. Sakurai, K. Okamoto, Z. Kawasaki, 2005: On the Relationship between Vertical Profile of Radar Reflectivity and Lightning Flash Rate Observed by the TRMM/PR and LIS, (in press).
Williams, E.R., 1985: Large Scale Charge Separation in Thunderclouds, *J. Geophys. Res.*, **90**, 6013-6025.
Williams, E., S. Rutledge, S. Geotis, N. Renno, E. Rasmussen and T. Rickenbach, 1992: A radar and electrical study of tropical 'hot towers', J. Atmos. Sci., 49, 1386-1395.
Williams, E.R. and N.O. Renno, 1993: An Analysis of the Conditional Instability of the Tropical Atmosphere, 121, 21-36.
Williams, E.R., 2001: The Electrification of Severe Storms, Chapter 13 in: Severe Convective Storms, AMS, Meteorological Monographs, **28**, Ed. C.A. Doswell, III, 561 pp.
Williams, E.R. and S. Stanfill, 2002: The Physical Origin of the Land-Ocean Contrast in Lightning Activity, Comptes Rendus—Physique, 3, 1277-1292, 2002.
Williams, E.R., and Coauthors, 2002: Contrasting Convective Regimes over the Amazon: Implications for Cloud Electrification, J. Geophys. Res., LBA Special Issue, 107, D20, 8082, doi:10.1029/2001JD000380.
Williams, E.R., 2005: Lightning and Climate: A Review, Atmospheric Research, 76, 272-287.
Williams, E., V. Mushtak, D. Rosenfeld, S. Goodman and D. Boccippio, 2005: Thermodynamic conditions favorable to superlative thunderstorm updraft, mixed phase microphysics and lightning flash rate, Atmos. Res., 76, 288-306.
Zipser, E.J., 2003: Some Views on "Hot Towers" after 50 years of Tropical Field Programs and Two Years of TRMM Data, Meteorological Monographs, 29, No. 51, 49-58.